DnaA modulates gene expression and morphology of the Lyme Disease spirochete

Andrew C. Krusenstjerna[1], Nerina Jusufovic[1], Timothy C. Saylor[1], Brian Stevenson[1,2]

1. Department of Microbiology, Immunology, and Molecular Genetics, University of Kentucky College of Medicine, Lexington, Kentucky, USA
2. Department of Entomology, University of Kentucky, Lexington, Kentucky, USA

Address for correspondence:

Department of Microbiology, Immunology, and Molecular Genetics

University of Kentucky, College of Medicine

Lexington, Ky. 40536-0278

Email: brian.stevenson@uky.edu

Phone: 1-859-257-9358

ABSTRACT.

All bacteria encode a multifunctional DNA-binding protein, DnaA, which initiates chromosomal replication. Despite having the most complex, segmented bacterial genome, little is known about *Borrelia burgdorferi* DnaA and its role in maintaining the spirochete's physiology. We utilized inducible CRISPR-interference and overexpression to modulate cellular levels of DnaA to better understand this essential protein. Dysregulation of DnaA, either up or down, significantly slowed replication and increased or decreased cell lengths. Using fluorescent microscopy, we found the DnaA CRISPRi mutants had increased numbers of chromosomes with irregular spacing patterns. The DnaA-depleted spirochetes also exhibited a significant defect in helical morphology. RNA-seq of the conditional mutants showed significant changes in the levels of transcripts involved with flagellar synthesis, elongation, cell division, virulence, and other functions. These findings demonstrate that the DnaA plays a commanding role in maintaining borrelial growth dynamics and protein expression, which are essential for the survival of the Lyme disease spirochete.

32 **Introduction.**

33 Replication plays a significant role in the enzootic lifecycle of *Borrelia burgdorferi*, the
34 Lyme disease spirochete. An obligate extracellular bacterial parasite, *B. burgdorferi* exclusively
35 colonizes Ixodid ticks and assorted vertebrates (1, 2). Naïve tick larvae acquire the Lyme bacteria
36 when they feed on an infected host. After this single blood meal, the larvae drop off, overwinter,
37 and molt to their nymphal stage. During this time, *B. burgdorferi* persists within the nutrient-
38 deplete tick midgut. Once the Ixodid nymph emerges and takes its blood meal, the spirochetes
39 obtain the requisite materials to replicate, divide, and disseminate from the tick to the vertebrate
40 host (3, 4).

41 The highly conserved AAA+ family protein DnaA initiates the replication of bacterial
42 chromosomes (5-7). DnaA monomers recognize the *oriC* and cooperatively multimerize to form a
43 helical structure. The DnaA filament promotes the separation of AT-rich DNA elements, which
44 recruits helicase and replication machinery. DnaA not only initiates chromosomal replication, but
45 it binds elsewhere in the genome to regulate gene expression (8, 9). We recently found the DnaA
46 of *B. burgdorferi* directly regulates the *dnaX-ebfC* operon, which codes for the Tau subunit of
47 DNA polymerase III holoenzyme, DnaX, and a regulatory nucleoid-associated protein, EbfC (10).
48 These genes are highly expressed during periods of rapid spirochete replication (10-12). At the
49 tick-vertebrate interface, we hypothesize that the *B. burgdorferi* DnaA not only commits to its
50 replication initiation function but coordinates the expression of genes needed for vertebrate
51 infection (10, 13, 14).

52 Replication of the *B. burgdorferi* linear chromosome proceeds bidirectionally from the
53 centrally-located *oriC* (15). Outside of this, little is known about borrelial DNA replication, its
54 regulation, or coordination with other cellular processes. Many of the genes involved in those

55 pathways are essential, which has hampered their investigation. Historically, studying essential
56 loci required the development or isolation of conditional mutants. The first studies into DnaA
57 utilized temperature-sensitive mutants (16). In the era of molecular genetics, many tools have been
58 developed to produce conditional phenotypes more readily, such as inducible promoters.
59 Overexpression has been a reliable means of elucidating a protein's function in *B. burgdorferi* and
60 other bacteria (14, 17, 18). Recently, inducible CRISPR interference (CRISPRi) systems have been
61 developed and added to the repertoire of tools for studying borrelial biology (19, 20). This work
62 will describe the consequence of CRISPRi-mediated knockdown of the essential replication
63 initiator protein DnaA in *B. burgdorferi*. Using this approach, coupled with overexpression, we
64 observed profound consequences of DnaA-dysregulation on spirochete morphology, chromosome
65 partitioning, and gene expression.

66 **RESULTS.**

67 **Construction and validation of plasmids to dysregulate levels of DnaA in *B.***
68 ***burgdorferi*.** DnaA is essential for initiating chromosomal replication, so deleting DnaA is lethal
69 to bacteria. Thus, to gain insight into the impacts of DnaA on borrelial physiology, we produced
70 IPTG-inducible constructs to reduce or elevate cellular levels of DnaA. Knockdown was carried
71 out using the newly refined all-in-one CRISPR interference (CRISPRi) shuttle vector, which
72 places the expression of both the sgRNA and a borrelial codon-optimized dCas9 gene under the
73 control of the Lac repressor (20). We designed two CRISPRi constructs with sgRNAs targeting
74 either the template ($dnaA_{T1}$) or non-template ($dnaA_{NT1}$) DNA strands directly 5' or within the *dnaA*
75 gene (**Fig. 1A**). Overexpression was achieved using plasmid pACK121, which contains an
76 inducible *dnaA* with an N-terminal 3xFLAG tag. All constructs were transformed into *B.*
77 *burgdorferi* strain B31-e2. The spirochetes tolerated each construct well, replicating at rates
78 comparable to the parental strain without the inducer (**Fig. 1B**), with one exception. The $dnaA_{T1}$
79 CRISPRi strain replicated slightly slower than the others, although it reached the same final density
80 as the others. This may suggest leakiness of the hybrid *lac* promoter that controls the sgRNA and
81 dCas9 gene (B. Murphy & W. Zückert, personal communication).

82 To assess the efficacy of these inducible constructs, spirochetes of each strain were grown
83 to mid-exponential growth phase (3-5x10^7 cells/ml), then incubated overnight with 0.5 mM IPTG.
84 The *dnaA*-targeting CRISPRi strains decreased the expression of DnaA, with the construct
85 targeting the template strand, $dnaA_{T1}$, consistently yielding the most effective gene silencing (**Fig.**
86 **1C** and **D**). The potency of the $dnaA_{T1}$ construct likely explains the slowed spirochete growth seen
87 in the absence of IPTG (**Fig. 1B**). Overexpression resulted in elevated quantities of DnaA protein
88 and transcript (**Fig. 1C** and **D**). Neither the CRISPRi empty vector (EV) nor the parental e2 control

89 strains yielded changes in DnaA levels when IPTG was added, demonstrating that we could
90 specifically and effectively alter cellular DnaA concentrations.

91 **Proper DnaA expression is essential for borrelial growth.** Given its essential nature for
92 chromosomal replication, we first sought to evaluate the consequence of DnaA dysregulation on
93 *B. burgdorferi* growth and cell division. To achieve this, all strains were grown to mid-exponential
94 phase and passaged into fresh media with 0.5 mM of IPTG at a density of $1x10^5$ cells/ml. Cultures
95 were counted every day for seven days to generate growth curves.

96 CRISPRi knockdown of DnaA levels substantially reduced the generation time and
97 carrying capacity of *B. burgdorferi* (**Fig. 2A** and **B**). The severity of these phenotypes was
98 consistent with the knockdown efficacy of the two constructs, with $dnaA_{NT1}$ cultures reaching a
99 maximum density that was one log lower and $dnaA_{T1}$ cultures maxing out two logs lower than the
100 controls. These data suggest that reducing the cellular concentration of DnaA directly limits the
101 number of division cycles, which is consistent with DnaA's role as the chromosomal replication
102 initiator.

103 Overproducing DnaA slowed growth during the first four days post-inoculation (dpi),
104 growing at a rate similar to the $dnaA_{T1}$ culture (**Fig. 2A** and **B,** early). After that time, however,
105 cultures consistently resumed logarithmic growth, yielding generation times that were
106 indistinguishable from the parental strain (**Fig. 2B**, late). We hypothesized this abrupt resumption
107 of growth was due to mutations in the inducible *dnaA* plasmid that eliminated overexpression. To
108 test this, we passaged spirochetes that had resumed growth into fresh media with IPTG to see if
109 growth would still be perturbed. Consistent with our hypothesis, these "conditioned" bacteria grew
110 at rates that were similar to the background strain (**Fig. 2C**), and induction of the 3xFLAG tagged
111 DnaA did not occur (**Fig. 2D**). To further test our hypothesis, we extracted the DnaA

112 overexpression plasmid from the *B. burgdorferi* cultures and transformed them into *E. coli*. We
113 sequenced purified plasmids from two colonies derived from the same induced borrelial culture.
114 Each clone had unique mutations within the *dnaA* ORF that truncated the full-length protein (**Fig.**
115 **2E**). Notably, both mutations resulted in the complete loss of domain IV, the DNA-binding domain
116 of DnaA. Plasmid isolated from *B. burgdorferi,* that had never been exposed to IPTG, did not have
117 any mutations within the inducible *dnaA*. These escape mutants, taken with the growth dynamics,
118 highlight the stressful nature of *dnaA* overexpression, which has consistently been observed in
119 other bacterial organisms (21-23).

120 Unlike the overexpression strain, we never observed a resumption of growth in the induced
121 *dnaA* CRISPRi strains. Furthermore, normal growth was attainable from knocked-down cultures
122 after passing spirochetes into fresh media without IPTG. These collective data demonstrate that
123 precisely controlled levels of DnaA are required for optimal borrelial growth *in vitro.*

124 **DnaA affects spirochete cell division/elongation.** Chromosomal replication is intimately
125 tied to cellular elongation and division (24-26). Having found that the conditional DnaA mutants
126 had replication defects, we also sought to assess the impact of DnaA dysregulation on *B.*
127 *burgdorferi* cell length. Over seven days, we imaged and measured spirochetes. In the parental e2
128 cultures, we observed a consistent pattern wherein median cell length peaked during early
129 exponential phase, followed by a steady decrease, then stabilization once the cultures reached
130 stationary phase (**Fig. 3A**, **3E,** and **3I**).

131 These findings sharply contrast with what we observed in the CRISPRi knockdown strains,
132 where the spirochetes steadily maintained median lengths of 30-40 µm (**Fig. 3B-C**, **3F**, **3H**, and
133 **3I**); the parental strain had median lengths that spanned from 24-32 µm. The ranges (maximum-

134 minimum) of the cell lengths within these knockdown strains (147 µm, *dnaA*$_{T1}$; 134 µm, *dnaA*$_{NT1}$)
135 were greater than that of the overexpression (77 µm) and parental (101 µm) bacteria.

136 When DnaA was overexpressed, the median cell length decreased after 2 dpi but gradually
137 increased to its peak at 5 dpi (**Fig. 3D**, **3H**, and **3J**). As the overexpressed cultures approached
138 peak densities, the cell lengths decreased. This oscillation in spirochete length aligned with the
139 observed growth pattern of this mutant, where slowed replication corresponds to cells of shorter
140 size and rapid replication to longer. This suggests that high levels of DnaA can diminish borrelial
141 cell length. Overall, these results demonstrate that DnaA plays a role in maintaining *B. burgdorferi*
142 cell elongation and/or division and that maintenance of proper DnaA levels is critical to these
143 processes.

144 **Impact of DnaA on ploidy and partitioning.** *B. burgdorferi* is polyploid during
145 exponential growth *in vitro* (27). As DnaA is the master initiator of chromosomal replication and
146 affects *B. burgdorferi* morphology, we hypothesized the ploidy and partitioning of the
147 chromosomes could be altered when DnaA levels are depleted. To test this, we transformed the
148 parental e2 and *dnaA*$_{T1}$ strains with a construct expressing the chromosomal ParB protein fused to
149 mCherry (pBSV2G_P$_{0826}$-mCherry$_{Bb}$-ParB), which has been demonstrated to bind near the *oriC*
150 (27). We first grew the two strains to mid-exponential phase without IPTG and measured the length
151 and ParB-*oriC* puncta per cell. The parental bacteria were smaller than those of the uninduced
152 *dnaA*$_{T1}$, consistent with our prior observations. Yet, both strains had similar numbers of ParB-*oriC*
153 (**Fig. 4**). After taking these measurements, the *dnaA*$_{T1}$ culture was split in half, and IPTG was
154 added to one of the cultures. The parental, uninduced, and induced strains were then incubated and
155 measured for three more days.

156 On the first day post-induction, as the cultures entered stationary phase (≥1x10^8 cells/ml),
157 all strains experienced a dramatic decline in the total ParB-*oriC* puncta per cell, consistent with
158 prior observations (27). Over the next two days, the number of these continued to decrease in the
159 parental and uninduced cultures, whereas the induced culture plateaued and ended with
160 significantly more ParB-*oriC* puncta. Furthermore, the induced cell lengths, while longer than the
161 parental, were the same as the uninduced cells, indicating the difference in puncta wasn't simply
162 due to differences in cell length. With this, we concluded that depleting DnaA impairs the
163 completion of borrelial chromosomal replication and cell division.

164 In addition to differences in the number of ParB-*oriC* puncta in the *dnaA*-conditional
165 mutant, we also noted an apparent difference in their spacing (**Fig. 5A-B**) relative to the parental
166 strain (**Fig. 5C**). Some cells had wide gaps between the foci, while others had foci that were close
167 together. We assessed the cultures two- and three-days post-induction and found about 23.7% of
168 parental e2 cells had irregular puncta spacing. The *dnaA*$_{T1}$ CRISPRi strains, in contrast, had
169 significantly greater proportions of 53.8% and 55.3% of spirochetes with irregular spacing without
170 and with added IPTG, respectively (**Fig. 5D**). Thus, knocking down DnaA also perturbs
171 chromosomal partitioning.

172 **Dysregulation of DnaA disrupts flagellar homeostasis.** Depletion of DnaA also resulted
173 in *B. burgdorferi* cells with aberrant helicity. Specifically, we observed spirochetes with a
174 complete or partial loss of their characteristic corkscrew shape (**Fig. 6A** and **B**, respectively). Some
175 of these tube-shaped cells were substantially elongated and showed evidence of incomplete
176 division (**Fig. 6C** and **Supplemental Video**). About 13% of the spirochetes in the *dnaA*$_{T1}$-induced
177 cultures and 8.7% of the uninduced exhibited these abnormal morphologies (**Fig. 6D**). The parental
178 and empty vector strains, independent of IPTG, did not exhibit such elevated proportions of these

179 cells, indicating that the observed helical abnormalities were due to targeted silencing of the *dnaA*
180 gene. The high level of abnormal cells in the uninduced *dnaA*$_{T1}$ cultures, relative to the controls,
181 can again be explained by leaky expression of the *dnaA* sgRNA encoded in the CRISPRi construct.

182 The characteristic corkscrew appearance of *B. burgdorferi* is due to the 7-11 flagella found
183 in the periplasm (28). The motors that direct the movement of the endoflagella are normally
184 localized to the bacterium's poles (29). The observed impacts on growth and partitioning suggest
185 coordination between replication and flagellar assembly at the sites of division. A connection
186 between DnaA and flagellar regulation has been observed in *E. coli* (30, 31).

187 **DnaA is a global regulator of borrelial gene expression.** DnaA is well known to be a
188 transcription factor in other bacteria, with regulons driving specific phenotypes (9). We have
189 previously demonstrated that the *B. burgdorferi* DnaA can control the expression of the *dnaX-ebfC*
190 operon (10). Considering this and the dramatic impacts of DnaA dysregulation on the Lyme
191 spirochete, we queried whether the myriad phenotypes of the conditional mutants are due to DnaA-
192 dependent transcriptional effects. To address this question, we performed RNA-seq on three strains
193 with different levels of DnaA enrichment: wild-type (e2), DnaA-up (e2 + pACK121), and DnaA-
194 down (e2 + *dnaA*$_{T1}$). All the strains had the plasmids cp26, lp17, lp54, cp32-1, cp32-3, cp32-4,
195 and cp32-7, as assessed by PCR and whole genome sequencing. The bacteria for RNA-seq analysis
196 were grown to mid-exponential phase, induced with 0.5 mM IPTG, and incubated overnight. We
197 chose this strategy to mitigate the chance of escape-mutant development from confounding the
198 results.

199 For the analyses of the RNA-seq data, comparisons were made between the three groups.
200 We considered a gene to be differentially expressed if the false discovery rate (FDR) was less than
201 or equal to 0.05 and had a $\log_2$FC (fold change) of ≥ 1 or ≤ -1. With these thresholds, 245 genes

202 were noted as being differentially expressed between the wild-type and DnaA-down cultures (79
203 down, 166 up; **Fig. 7A**), 88 genes between WT and DnaA-up (40 down, 48 up; **Fig. 7B**), and 283
204 between DnaA-down and DnaA-up (108 down, 175 up; **Fig. 7C**). Principle component analysis
205 showed that the replicates of each strain clustered together (**Fig. 7D**). Most of the genes that were
206 differentially expressed are encoded on the chromosome: DnaA-down/e2: 61.6%; DnaA-up/e2:
207 68.2% (**Fig. 7E**). Of the plasmids, the circular cp32-7 replicon had the most impacted genes for
208 the DnaA-down/e2 and DnaA-up/e2 comparisons, 12.2% and 6.8%, respectively (**Fig. 7E**).

209 As expected, compared to the e2 parent, *dnaA* transcript was about 2.8-fold less abundant
210 in the CRISPRi strain and 15-fold more abundant in the overexpression strain, qRT-PCR validated
211 this pattern. Using *ftsK* for normalization, about 17-fold less *dnaA* transcript was detected in the
212 knockdown strain vs WT, and there was about 33-fold more in the overexpression (**Fig. 7E**). Since
213 *ftsK* was also impacted by *dnaA* dysregulation (discussed below), we normalized to *rpoB*, which
214 did not change under these conditions. Using this approach, *dnaA* transcript was 80-fold less
215 abundant in the knockdown vs. the WT and 16-fold more abundant in the overexpression vs the
216 WT (**Fig. 7E**). DnaA protein levels were about half as abundant in the knockdown and 13 times
217 more in overexpression than the WT (**Fig. 10B**).

218 The transcripts of many genes were most affected when *dnaA* levels were reduced. We
219 initially hypothesized that transcriptomic profiles between the conditional mutants relative to the
220 parental strain would reciprocally mirror each other. Only two genes fit this pattern: *dnaA*, which
221 was expected, and BB_0413 (2.2-fold increase for $dnaA_{T1}$/e2; 2.4-fold decrease for 121/e2).
222 Indeed, in many cases, transcript levels for a gene would experience the same degree of change
223 regardless of whether DnaA was increased or decreased. Such instances suggested that some of
224 the observed changes in gene expression were not due to DnaA itself but rather a shared cellular

225 response to the change in WT DnaA levels. Despite some of these complications, the RNA-seq
226 data set offered interesting insights into the phenotypes observed in the conditional *dnaA*-mutant
227 strains.

228 The earliest interrogations into borrelial DnaA focused on its function as a transcription
229 factor (10, 14). Consistent with our prior *in vitro* studies, knocking down *dnaA* significantly
230 decreased transcription of the *dnaX-ebfC* operon (10). This operon codes for the τ-subunit of the
231 DNA polymerase III holoenzyme (DnaX) and the nucleoid-associated protein, EbfC. Other
232 impacted replication genes included the DNA polymerase III β-clamp (*dnaN*), DNA polymerase I
233 (*polA*), DNA topoisomerase IV (*parEC*), and telomere resolvase (*resT*). Except for *dnaN*, these
234 genes were downregulated when *dnaA* levels were decreased. The upregulation of *dnaN*, seen
235 when comparing DnaA-Up to DnaA-down conditions, suggests that DnaA represses the
236 expression of this gene. This possibility is unsurprising given that the *oriC* is directly 5' of the
237 *dnaN* ORF, and we have shown that DnaA binds this region (10).

238 In the *dnaA*-knockdown *B. burgdorferi*, we observed cells that were considerably
239 elongated. In our evaluation of the borrelial genome, we identified 22 homologs of genes that
240 encode components of either the bacterial elongasome or divisome (**Table 1**). Of these, 39.1%
241 were differentially expressed in the *dnaA*$_{T1}$ CRISPRi strain (**Fig. 8A**). Among these were *mreB*,
242 *mreC*, *mreD,* and *mrdA*, which constitute an apparent operon and encode core components of the
243 bacterial elongasome (**Fig. 8B**). MreB is an actin-like cytoskeleton protein that polymerizes across
244 the bacterial inner membrane to regulate the spatiotemporal peptidoglycan synthesis of growing
245 cells (32-34). Knockdown of MreB in *B. burgdorferi* results in bulging and cell widening at the
246 division sites (19). MreC and MreD are membrane-embedded proteins that interact and regulate
247 the peptidoglycan crosslinking activity of PBP2 (penicillin-binding protein 2; MrdA) (35). The

248 peptidoglycan polymerase RodA and PBP1a interact with PBP2, with the former stimulating its
249 activity. Except for *mreD*, the genes in the apparent *mre* operon were downregulated in *dnaA*-
250 deficient *B. burgdorferi*. A DNA sequence that is the same as those found in the *oriC*, which may
251 constitute the borrelial DnaA-box, is located upstream of the *mreB* ORF, suggesting DnaA may
252 directly regulate the expression of these genes. The decreased transcript levels for *mreB*, *mreC*,
253 and *mrdA* would suggest decreased elongation, which is the opposite of what we observed (**Fig.**
254 **3**). This apparent contradiction suggests that filamentation may be due to defects in cell division.

255 The transcripts of four important divisome proteins were impacted when *dnaA* was
256 knocked down: FtsA, FtsK, FtsE, and FtsX (**Fig. 8A** and **B**). FtsA is the membrane anchor protein
257 for the septation marker protein FtsZ (36, 37), and its transcript increased about 2-fold in the
258 conditional *dnaA* mutant. Interestingly, DnaA-overexpressed *B. burgdorferi* also had 2-fold
259 increased levels of *ftsA* transcript. Transcripts for FtsK, the DNA translocase, declined 2-fold. FtsE
260 and FtsX, encoded next to each other, had their transcripts decreased 2-fold and increased almost
261 3-fold, respectively. Interestingly, a second copy of *ftsX*, which is truncated, is located directly
262 upstream of *ftsEX,* and transcript levels of this gene were substantially affected, with a 187-fold
263 increase. Like the *mre* locus, DnaA could regulate these genes directly as there are potential DnaA-
264 boxes adjacent to these loci.

265 In the conditional *dnaA*-knockdown *B. burgdorferi,* we observed spirochetes that had lost
266 their helical structure and hypothesized these cells had disrupted flagella. The *B. burgdorferi*
267 genome encodes nearly three dozen flagellar genes (**Fig. 9A**). When *dnaA* was knocked down,
268 five of these genes were impacted: *fliQ*, *fliR*, *flgD*, *flgV*, and *flgA* (**Fig. 9B***)*. All these genes except
269 *flgA* are encoded in the *flgB* superoperon. FliQ and FliR are components of the flagellar export
270 apparatus (38). FlgD is a scaffolding protein that is required for flagellar hook formation (39, 40).

271 FlgV is a protein that was first annotated as an Hfq homolog, but recent work has demonstrated
272 the protein localizes with the flagellar motor and modulates its assembly (41, 42). FlgA is a
273 chaperone involved in the formation of the P-ring of the flagellar motor (43). The transcripts for
274 *fliR* and *flgD* increased the most of these genes, about 15 and 4-fold, respectively, when DnaA
275 levels were reduced. The changes in expression of these genes could perhaps alter flagellar
276 assembly homeostasis and explain the observed abnormalities in helicity in the *dnaA*-deficient
277 spirochetes. It is also possible that septation defects disrupted the localization and assembly of
278 flagella.

279 In addition to affecting genes for essential cellular processes, DnaA appears to regulate the
280 expression of outer surface proteins involved in Lyme pathogenesis, such as ErpA, ErpM, decorin
281 binding protein DbpA, and OspC (**Fig. 7A-C** and **Fig. 10E-F**). The Erps are multifunctional
282 adhesins that bind vertebrate host factors laminin, plasminogen, and complement proteins (44-49).
283 Interestingly, *erpA* and *erpM* transcripts increased in the *dnaA* knockdown and overexpression
284 conditions (**Fig. 10E-F**). While the increase in transcript didn't correspond to significantly
285 increased ErpA protein levels, ErpM increased 2-fold in the DnaA-knockdown condition (**Fig.**
286 **10B-D**)

287 The *erp* genes are encoded on the cp32 plasmids and have conserved operators that allow
288 for uniform regulation (50). The Erps are turned on when the tick begins to feed, a time of rapid
289 borrelial replication, and remain on during vertebrate infection (51). Three proteins bind the *erp*
290 operators and regulate their expression: BpaB (Borrelial cp32 ParB analog), BpuR, and EbfC.
291 BpaB represses *erp* transcription along with the co-repressor BpuR (**Fig. 10A**) (52-54). EbfC is
292 the antirepressor that antagonizes BpaB to allow for *erp* transcription (53). DnaA is thought to
293 regulate the Erps by activating EbfC and repressing BpuR (10, 13, 14). EbfC transcript and protein

294 levels decreased when *dnaA* was knocked down, consistent with that model (**Fig. 10B** and **E**).
295 BpuR transcript, however, did not significantly change, but its protein levels appeared to decline
296 with a decrease in cellular DnaA concentrations (**Fig. 10B** and **E**). BpuR alone does not repress
297 *erp* expression, so this cannot account for the increase in ErpA and ErpM. Thus, we decided to
298 look at levels of the *erp* repressor. Despite the lack of a change in the transcript, immunoblots
299 showed a decrease in BpaB protein levels in the *dnaA* CRISPRi *B. burgdorferi*, which can explain
300 the increase in Erp expression (**Fig. 10B, C,** and **E**). These results demonstrate that DnaA not only
301 affects the expression of genes involved in basic cellular processes but also those involved in
302 maintaining the Lyme spirochete's infection cycle.

303 **METHODS AND MATERIALS.**

304 **Bacterial strains, plasmids, and genetic manipulations.** Studies were conducted using
305 the readily transformable *B. burgdorferi* clonal strain B31-e2 (55). Spirochetes were grown in
306 liquid Barbour-Stoener-Kelly II (BSK-II) medium supplemented with 6% rabbit serum (v/v) at 35
307 ºC. For all experiments, *B. burgdorferi* was passed from mid-exponential phase (3-5 x 10^7 cells/ml)
308 into fresh BSK-II medium. Cultures were only used if they were at least two passages away and
309 no more than three from the initial stock. Borrelial culture densities were enumerated using a
310 Petroff-Hauser counting chamber and dark-field microscopy.

311 The *dnaA* overexpression (pACK121) and CRISPRi plasmids (pACK136, $dnaA_{T1}$;
312 pACK138, $dnaA_{NT1}$) were generated by GenScript. The pACK121 plasmid is a derivative of
313 pJSB268 (17). The plasmid was designed to replace the *luc* gene with the *B. burgdorferi dnaA*
314 gene containing an N-terminal 3xFLAG epitope. The pACK136 ($dnaA_{T1}$) and pACK137
315 ($dnaA_{NT1}$) plasmids are derivatives of pJJW101 (20). These plasmids were created by inserting the
316 desired sgRNA sequence between the BsaI sequences. The sgRNA targets used in this study were
317 chosen using CRISPy-web (https://crispy.secondarymetabolites.org) and B31 chromosome contig
318 (NC_001318). All plasmids were sequenced before use.

319 **Growth curve analysis.** Growth curves for each strain were generated from three
320 independent experiments. Generation times were calculated in Microsoft Excel by fitting an
321 exponential curve to the data points denoting the beginning and end of logarithmic growth.
322 Statistically significant differences were determined by one-way ANOVA.

323 **Immunoblot analyses.** Polyclonal DnaA antibodies were generated by Thermo Scientific
324 in rabbits using recombinant GST-DnaA (10). The serum from the final bleed was purified by
325 affinity purification using MBP-DnaA on an amylose column. Murine monoclonal anti-FlaB

326 antibodies were used to assess the even loading of SDS-PAGE gels (56). Cells for immunoblot
327 were pelleted and washed three times with 1x PBS, pH 7.4. Approximately 10^7 spirochetes were
328 loaded per lane for SDS-PAGE. Goat anti-Rabbit Alexa Fluor 488 (Thermo Scientific) and Goat
329 anti-Mouse IRDye800 (Licor) were used as secondary antibodies. Densitometric analyses were
330 performed using ImageLab software (BioRad). The intensities of the bands of interest were
331 normalized to the corresponding loading control.

332 **Quantitative reverse transcription-PCR (qRT-PCR).** Bacteria were washed three times
333 with PBS (pH 7.4) before RNA extraction using the Qiagen Mini RNA kit. Genomic DNA was
334 cleared by on-column DNase treatment. RNA was reverse transcribed using iScript gDNA Clear
335 cDNA synthesis kits (Bio-Rad). Quantitative PCR was conducted using iTaq Universal SYBR
336 Green Supermix (Bio-Rad) and Bio-Rad CFX96 Touch Real-time PCR thermocycler. The primer
337 sets used for this study were designed using the IDT Primer Quest Tool
338 (https://www.idtdna.com/PrimerQuest/Home/Index). Cq values were normalized to *ftsK* or *rpoB*
339 (ΔCq) and then to the parental strain or uninduced control (ΔΔCq). Fold expression was
340 determined using the function $2^{-\Delta\Delta Cq}$. If ΔΔCq > 0 then the function $-2^{\Delta\Delta Cq}$ was used.

341 **Cell length analysis.** Wet mounts of live bacteria were visualized by dark-field with an
342 Olympus Bx51 microscope. Micrographs were taken using a C-mounted Accu-scope Excelis HD
343 camera. Cell lengths were determined using Captavision+ software. A conversion factor of 13.80
344 pixels/µm was used for all measurements. For each replicate and time point, approximately 50
345 spirochetes were measured.

346 **Fluorescence microscopy and image analysis.** Spirochetes were pelleted by
347 centrifugation, washed twice with PBS (pH 7.4), and diluted to a final concentration of 1 x 10^5
348 cells/ml. Ten microliters of cells were mounted on a glass slide. Cells were visualized using an

349 Olympus Bx51 microscope with a Cool LED p-E300 illumination system. Micrographs of dark-
350 field and red fluorescence were captured for each field of view using a C-mounted Accu-scope
351 Excelis HD camera. Micrographs were merged in ImageJ, and the background was inverted using
352 EZreverse with the HSL color space option (57).

353 **RNA sequencing (RNA-seq) and analysis.** The parental *B. burgdorferi* e2, *dnaA*$_{T1}$
354 CRISPRi, and *dnaA*-overexpression strains were used for RNA-seq. All strains were grown in
355 duplicate to mid-exponential growth phase (3-5 x 10^7 cells/ml) and induced with 0.5 mM IPTG
356 overnight at 35 ºC. The cells were pelleted and washed two times with PBS (pH 7.4) and frozen at
357 -80 ºC. The cells were sent to SeqCenter for RNA extraction and sequencing using their
358 intermediate RNA analysis with replicates (Prokaryotic) service. Briefly, their method consisted
359 of quality control and adapter trimming by bclconvert (version 4.1.5) and mapping reads using
360 HISAT2 (version 2.2.0). The read counts were uploaded into R (version 4.0.2) and normalized
361 using the edgeR Trimmed Mean of M values (TMM) algorithm (1.14.5).

362 We further filtered the data set by setting the thresholds for differential expression at
363 $\log_2 FC \geq 1$ or ≤ -1 and an FDR < 0.5. Volcano plots were made using VolcaNoseR (58). The
364 heatmap was generated using SRPlot and the normalized read counts for genes with significant
365 differential expression (59).

366 To identify flagellar, cell division, and elongation homologs, the genome was directly
367 searched for annotations, or the sequences of characterized proteins from other bacteria were
368 aligned by BLAST against the *B. burgdorferi* genome.

369

370 **DISCUSSION**

371 In this study, we sought to understand the roles of DnaA in controlling the physiology of
372 *B. burgdorferi*. To do this, we utilized inducible CRISPRi and overexpression vectors.
373 Overexpressing DnaA was toxic to the bacteria and was consistently overcome by mutations in
374 the inducible *dnaA*. This, along with the difference in DnaA levels from overexpression vs.
375 knockdown, 13-fold DnaA increase vs. 2-fold decrease, likely explains some of the confounding
376 results we encountered. Nevertheless, increasing DnaA levels yielded some interesting
377 phenotypes, such as decreased spirochete size. CRISPRi was the more reliable and effective means
378 of producing conditional *dnaA* mutants in *B. burgdorferi*. This approach targeting *dnaA* has been
379 successfully described in *E. coli*, *Lactobacillus plantarum,* and *Streptococcus pyogenes* (60-62).
380 An attempt was made in *Pseudomonas putida,* but clones couldn't be recovered (63).

381 We found that lowering the cellular levels of DnaA profoundly reduced growth, consistent
382 with the protein's function as the chromosomal replication initiator. The reduction of DnaA also
383 coincided with decreased expression of many essential replication genes. It is known that one of
384 these genes, *dnaX*, is directly regulated by DnaA (10). This suggests that DnaA may directly
385 regulate those other genes, or *B. burgdorferi* may have mechanisms to sense replication initiation
386 and coordinate gene expression accordingly.

387 DnaA-deficient spirochetes also increased their length. The bacterial cell cycle is typically
388 divided into three phases: B, C, and D (64). The B and D phases correspond to the birth and
389 division of the bacteria, respectively. The C phase corresponds to everything in between, namely,
390 chromosomal replication, but elongation/growth as well. Replication is initiated by DnaA and then
391 carried out by the replisome. Elongation is facilitated by the elongasome, which synthesizes
392 peptidoglycan to allow for cell growth. The DnaA-depleted spirochetes, although considerably

393 longer than the parental strain, had overall decreased expression of elongasome genes, the *mre*
394 locus in particular. This suggested a division issue, but we cannot rule out the possibility that
395 DnaA is required for cross-talk between replication and cell growth. Indeed, it is likely that
396 replication, elongation, and division are all interconnected. Lyme and relapsing *Borreliae* elongate
397 at three distinct zones along their length: 1/4, 1/2, and 3/4 (65). This localization pattern at the
398 mid-cell suggests an interplay between elongation and division machinery. How or if DnaA
399 directly plays into this delicate balance remains to be assessed.

400 Many bacterial cell division proteins are denoted "Fts" for their filamentous phenotypes
401 caused by temperature-sensitive mutations (66). Knocking down DnaA affected the expression of
402 *ftsA*, *ftsEX*, and *ftsK*. The dysregulation of these genes potentially explains both the elongated
403 phenotype and the irregular spacing of the ParB-*oriC* puncta.

404 FtsA localizes to the inner leaflet of the inner membrane and binds FtsZ. Increased FtsA,
405 seen when DnaA was knocked down, could decrease Z-ring assembly and, thus, cytokinesis. In *E.*
406 *coli*, overexpression of FtsA causes cells to filament (67). Overexpressed DnaA spirochetes had
407 elevated *ftsA* transcript, but no changes were observed in *ftsEX*. The FtsEX complex regulates the
408 activity of peptidoglycan hydrolases and FtsA (68-71). Disruption of FtsE and FtsX levels could,
409 therefore, prevent the breakdown of peptidoglycan and Z-ring formation at the site of division.
410 The combined perturbation of *ftsA* and *ftsEX* expression in the *dnaA* CRISPRi strain potentially
411 explains the observed elongated phenotype.

412 In addition to changes in spirochete length in the DnaA-depleted *B. burgdorferi*, we
413 observed abnormal spacing of ParB-*oriC* puncta. These bacteria had decreased transcripts of the
414 membrane-embedded DNA translocase FtsK, a core component of the divisome (72-74). FtsK,
415 through its C-terminal αβγ-domain, resolves chromosome dimers and translocates DNA from the

416 septum to allow for cytokinesis (75-78). A decrease in FtsK could thus result in the failure to
417 separate sister chromosomes, leading to cells with abnormal ploidy. This could also explain why
418 some *oriC* sites were located close together in the *dnaA* knockdown strain (**Fig. 5**). FtsK also
419 recruits downstream divisome proteins through its N-terminal transmembrane domain (73, 79-81).
420 Therefore, reducing FtsK may limit the recruitment of divisome proteins to the septa.

421 Motility is perhaps the most important "virulence" factor that *B. burgdorferi* employs to
422 infect and colonize its vertebrate hosts. By knocking down DnaA in the Lyme spirochete, we
423 observed a substantial impact on the bacteria's helicity. This corkscrew morphology is due to
424 periplasmic flagella (28). Key genes, such as FlgD and FliR, were overexpressed when levels of
425 DnaA were lowered. FliR is a component of the flagellar motor's export apparatus, which
426 transports flagellar filament substrates from the cytoplasm to the periplasm (38). Disrupting the
427 balance of this subunit would very likely impair the overall function and structure of the flagellar
428 motor and filament. By increasing FliR, it is possible that the export of the flagellar cargo to the
429 periplasmic space would be affected, which in turn would prevent flagella formation. The flagellar
430 motors are mostly localized to the poles of *B. burgdorferi*. This suggests that replication,
431 elongation, or division processes may coordinate the formation of flagellar motors at the dividing
432 mid-cell. In *E. coli*, DnaA regulates genes involved in flagellar assembly (30, 31, 82). Whether
433 DnaA in *B. burgdorferi* acts through a similar mechanism is unknown.

434 In addition to the many morphological changes incurred by dysregulation of DnaA, there
435 were also significant impacts on the expression of vertebrate infection-related outer surface
436 proteins. Many of these antigenic proteins, such as the Erps, decorin binding proteins DbpA, and
437 OspC, are turned on during the tick blood meal, a period defined by rapid replication. Relative to
438 these genes, levels of transcript for the alternative sigma factor RpoS were not significant by

439 manipulation of DnaA levels. We previously demonstrated that DnaA regulates the *erp*
440 antirepressor EbfC and may regulate the *erp* co-repressor BpuR (10, 14). With our CRISPRi
441 approach, we were able to validate our prior data on *dnaX-ebfC* regulation. While we could not
442 detect any substantial differences in BpuR with DnaA manipulation, this is likely a consequence
443 of assessing mid-exponential spirochetes grown at 34 ºC; BpuR expression is highest when grown
444 at 23 ºC (14, 54). When DnaA levels were reduced, expression of ErpA and ErpM increased. We
445 suggest this could be due to decreased levels of *erp* repressor BpaB. While this was unexpected, it
446 is logical that a partitioning protein be decreased when *dnaA* transcription is knocked down. This
447 suggests that these extrachromosomal DNAs can sense changes in chromosomal replication. How
448 this is mediated remains to be investigated.

449 Organisms have evolved complex and varied molecular circuits to regulate cellular
450 homeostasis in ever-changing environments. Bacterial pathogens, especially, have developed such
451 networks in their tussle against host defenses. During the tick blood meal, *B. burgdorferi* must take
452 advantage of the nutrients to propagate its numbers, reprogram its transcriptome, and disseminate
453 to the vertebrate. Failure to do so means death, as *B. burgdorferi* cannot be transmitted vertically
454 to tick offspring (83). In *B. burgdorferi,* DnaA, the master regulator of replication initiation,
455 appears to form a complex regulatory network to coordinate these essential processes. Future
456 studies need to be conducted to determine which of the DnaA-dysregulated effects described here
457 are due to DnaA itself or a consequence of a lack of initiation of chromosomal replication.

Acknowledgments

This research was funded by NIH grant R21 AI147139. We thank Dr. Wolfram Zückert and Bryan Murphy for their help designing and troubleshooting the CRISPRi shuttle vectors and Dr. Jon Blevins for providing the pJSB268 shuttle vector. BioRender was used to make the schematics in Figures 1, 2, 8, 9, and 10.

463 **Works Cited.**

464 1. Radolf JD, Caimano MJ, Stevenson B, Hu LT. 2012. Of ticks, mice and men:
465 understanding the dual-host lifestyle of Lyme disease spirochaetes. Nat Rev Microbiol
466 10:87-99.
467 2. Steere AC, Strle F, Wormser GP, Hu LT, Branda JA, Hovius JW, Li X, Mead PS. 2016.
468 Lyme borreliosis. Nat Rev Dis Primers 2:16090.
469 3. De Silva AM, Fikrig E. 1995. Growth and migration of *Borrelia burgdorferi* in *Ixodes*
470 ticks during blood feeding. Am J Trop Med Hyg 53:397-404.
471 4. Piesman J, Oliver JR, Sinsky RJ. 1990. Growth kinetics of the Lyme disease spirochete
472 (*Borrelia burgdorferi*) in vector ticks (*Ixodes dammini*). Am J Trop Med Hyg 42:352-7.
473 5. Speck C, Messer W. 2001. Mechanism of origin unwinding: sequential binding of DnaA
474 to double- and single-stranded DNA. EMBO J 20:1469-76.
475 6. Kaur G, Vora MP, Czerwonka CA, Rozgaja TA, Grimwade JE, Leonard AC. 2014.
476 Building the bacterial orisome: high-affinity DnaA recognition plays a role in setting the
477 conformation of *oriC* DNA. Mol Microbiol 91:1148-63.
478 7. Ozaki S, Katayama T. 2012. Highly organized DnaA-*oriC* complexes recruit the single-
479 stranded DNA for replication initiation. Nucleic Acids Res 40:1648-65.
480 8. Messer W, Weigel C. 1997. DnaA initiator--also a transcription factor. Mol Microbiol
481 24:1-6.
482 9. Menikpurage IP, Woo K, Mera PE. 2021. Transcriptional Activity of the Bacterial
483 Replication Initiator DnaA. Front Microbiol 12:662317.

484 10. Krusenstjerna AC, Saylor TC, Arnold WK, Tucker JS, Stevenson B. 2023. *Borrelia*
485 *burgdorferi* DnaA and the Nucleoid-Associated Protein EbfC Coordinate Expression of
486 the *dnaX-ebfC* Operon. J Bacteriol 205:e0039622.
487 11. Medrano MS, Ding Y, Wang X-G, Lu P, Coburn J, Hu LT. 2007. Regulators of
488 expression of the oligopeptide permease A proteins of *Borrelia burgdorferi*. Journal of
489 bacteriology 189:2653-2659.
490 12. Jutras BL, Bowman A, Brissette CA, Adams CA, Verma A, Chenail AM, Stevenson B.
491 2012. EbfC (YbaB) is a new type of bacterial nucleoid-associated protein and a global
492 regulator of gene expression in the Lyme disease spirochete. J Bacteriol 194:3395-406.
493 13. Stevenson B, Krusenstjerna AC, Castro-Padovani TN, Savage CR, Jutras BL, Saylor TC.
494 2022. The Consistent Tick-Vertebrate Infectious Cycle of the Lyme Disease Spirochete
495 Enables Borrelia burgdorferi To Control Protein Expression by Monitoring Its
496 Physiological Status. J Bacteriol 204:e0060621.
497 14. Jutras BL, Savage CR, Arnold WK, Lethbridge KG, Carroll DW, Tilly K, Bestor A, Zhu
498 H, Seshu J, Zuckert WR, Stewart PE, Rosa PA, Brissette CA, Stevenson B. 2019. The
499 Lyme disease spirochete's BpuR DNA/RNA-binding protein is differentially expressed
500 during the mammal-tick infectious cycle, which affects translation of the SodA
501 superoxide dismutase. Mol Microbiol 112:973-991.
502 15. Picardeau M, Lobry JR, Hinnebusch BJ. 1999. Physical mapping of an origin of
503 bidirectional replication at the centre of the *Borrelia burgdorferi* linear chromosome. Mol
504 Microbiol 32:437-45.

505 16. Hirota Y, Ryter A, Jacob F. 1968. Thermosensitive mutants of *E. coli* affected in the
506 processes of DNA synthesis and cellular division. Cold Spring Harb Symp Quant Biol
507 33:677-93.
508 17. Blevins JS, Revel AT, Smith AH, Bachlani GN, Norgard MV. 2007. Adaptation of a
509 luciferase gene reporter and *lac* expression system to *Borrelia burgdorferi*. Appl Environ
510 Microbiol 73:1501-13.
511 18. Groshong AM, Gibbons NE, Yang XF, Blevins JS. 2012. Rrp2, a prokaryotic enhancer-
512 like binding protein, is essential for viability of *Borrelia burgdorferi*. J Bacteriol
513 194:3336-42.
514 19. Takacs CN, Scott M, Chang Y, Kloos ZA, Irnov I, Rosa PA, Liu J, Jacobs-Wagner C.
515 2020. A CRISPR interference platform for selective downregulation of gene expression
516 in *Borrelia burgdorferi*. Appl Environ Microbiol doi:10.1128/AEM.02519-20.
517 20. Murphy BT, Wiepen JJ, He H, Pramanik AS, Peters JM, Stevenson B, Zuckert WR.
518 2023. Inducible CRISPRi-Based Operon Silencing and Selective in Trans Gene
519 Complementation in *Borrelia burgdorferi*. J Bacteriol 205:e0046822.
520 21. Zheng W, Li Z, Skarstad K, Crooke E. 2001. Mutations in DnaA protein suppress the
521 growth arrest of acidic phospholipid-deficient *Escherichia coli* cells. EMBO J 20:1164-
522 72.
523 22. Jonas K, Chen YE, Laub MT. 2011. Modularity of the bacterial cell cycle enables
524 independent spatial and temporal control of DNA replication. Curr Biol 21:1092-101.
525 23. Anderson ME, Smith JL, Grossman AD. 2022. Multiple mechanisms for overcoming
526 lethal over-initiation of DNA replication. Mol Microbiol 118:426-442.

527 24. Cooper S, Helmstetter CE. 1968. Chromosome replication and the division cycle of
528 *Escherichia coli* Br. Journal of Molecular Biology 31:519-540.
529 25. Donachie WD. 1968. Relationship between Cell Size and Time of Initiation of DNA
530 Replication. Nature 219:1077-1079.
531 26. Wallden M, Fange D, Lundius EG, Baltekin Ö, Elf J. 2016. The Synchronization of
532 Replication and Division Cycles in Individual *E. coli* Cells. Cell 166:729-739.
533 27. Takacs CN, Wachter J, Xiang Y, Ren Z, Karaboja X, Scott M, Stoner MR, Irnov I,
534 Jannetty N, Rosa PA, Wang X, Jacobs-Wagner C. 2022. Polyploidy, regular patterning of
535 genome copies, and unusual control of DNA partitioning in the Lyme disease spirochete.
536 Nat Commun 13:7173.
537 28. Motaleb MA, Corum L, Bono JL, Elias AF, Rosa P, Samuels DS, Charon NW. 2000.
538 *Borrelia burgdorferi* periplasmic flagella have both skeletal and motility functions. Proc
539 Natl Acad Sci U S A 97:10899-904.
540 29. Li C, Bakker RG, Motaleb MA, Sartakova ML, Cabello FC, Charon NW. 2002.
541 Asymmetrical flagellar rotation in *Borrelia burgdorferi* nonchemotactic mutants. Proc
542 Natl Acad Sci U S A 99:6169-74.
543 30. Wu D, Baigalmaa L, Yao Y, Li G, Su M, Fan L, Morigen. 2021. The *Escherichia coli*
544 QseB/QseC signaling is required for correct timing of replication initiation and cell
545 motility. Gene 773:145374.
546 31. Mizushima T, Tomura A, Shinpuku T, Miki T, Sekimizu K. 1994. Loss of flagellation in
547 *dnaA* mutants of *Escherichia coli*. J Bacteriol 176:5544-6.
548 32. Jones LJ, Carballido-Lopez R, Errington J. 2001. Control of cell shape in bacteria:
549 helical, actin-like filaments in *Bacillus subtilis*. Cell 104:913-22.

550 33. Kruse T, Bork-Jensen J, Gerdes K. 2005. The morphogenetic MreBCD proteins of
551 *Escherichia coli* form an essential membrane-bound complex. Mol Microbiol 55:78-89.
552 34. Figge RM, Divakaruni AV, Gober JW. 2004. MreB, the cell shape-determining bacterial
553 actin homologue, co-ordinates cell wall morphogenesis in *Caulobacter crescentus*. Mol
554 Microbiol 51:1321-32.
555 35. Liu X, Biboy J, Consoli E, Vollmer W, den Blaauwen T. 2021. MreC and MreD balance
556 the interaction between the elongasome proteins PBP2 and RodA. PLOS Genetics
557 16:e1009276.
558 36. Pichoff S, Lutkenhaus J. 2005. Tethering the Z ring to the membrane through a conserved
559 membrane targeting sequence in FtsA. Mol Microbiol 55:1722-34.
560 37. Pichoff S, Lutkenhaus J. 2002. Unique and overlapping roles for ZipA and FtsA in septal
561 ring assembly in *Escherichia coli*. Embo j 21:685-93.
562 38. Minamino T, Macnab RM. 1999. Components of the *Salmonella* flagellar export
563 apparatus and classification of export substrates. J Bacteriol 181:1388-94.
564 39. Kutsukake K, Doi H. 1994. Nucleotide sequence of the *flgD* gene of *Salmonella*
565 *typhimurium* which is essential for flagellar hook formation. Biochim Biophys Acta
566 1218:443-6.
567 40. Ohnishi K, Ohto Y, Aizawa S, Macnab RM, Iino T. 1994. FlgD is a scaffolding protein
568 needed for flagellar hook assembly in *Salmonella typhimurium*. J Bacteriol 176:2272-81.
569 41. Lybecker MC, Abel CA, Feig AL, Samuels DS. 2010. Identification and function of the
570 RNA chaperone Hfq in the Lyme disease spirochete *Borrelia burgdorferi*. Mol Microbiol
571 78:622-35.

572 42. Zamba-Campero M, Soliman D, Yu H, Lasseter AG, Chang Y-Y, Liu J, Aravind L,
573 Jewett MW, Storz G, Adams PP. 2024. Broadly conserved FlgV controls flagellar
574 assembly and *Borrelia burgdorferi* dissemination in mice. bioRxiv
575 doi:10.1101/2024.01.09.574855:2024.01.09.574855.
576 43. Juhas M, Ajioka JW. 2015. Identification and validation of novel chromosomal
577 integration and expression loci in *Escherichia coli* flagellar region 1. PLoS One
578 10:e0123007.
579 44. Stevenson B, Brissette CA. 2023. Erp and Rev Adhesins of the Lyme Disease
580 Spirochete's Ubiquitous cp32 Prophages Assist the Bacterium during Vertebrate
581 Infection. Infect Immun 91:e0025022.
582 45. Stevenson B, El-Hage N, Hines MA, Miller JC, Babb K. 2002. Differential binding of
583 host complement inhibitor factor H by *Borrelia burgdorferi* Erp surface proteins: a
584 possible mechanism underlying the expansive host range of Lyme disease spirochetes.
585 Infect Immun 70:491-7.
586 46. Brissette CA, Haupt K, Barthel D, Cooley AE, Bowman A, Skerka C, Wallich R, Zipfel
587 PF, Kraiczy P, Stevenson B. 2009. *Borrelia burgdorferi* infection-associated surface
588 proteins ErpP, ErpA, and ErpC bind human plasminogen. Infect Immun 77:300-6.
589 47. Brissette CA, Verma A, Bowman A, Cooley AE, Stevenson B. 2009. The *Borrelia*
590 *burgdorferi* outer-surface protein ErpX binds mammalian laminin. Microbiology
591 (Reading) 155:863-872.
592 48. Garrigues RJ, Thomas S, Leong JM, Garcia BL. 2022. Outer surface lipoproteins from
593 the Lyme disease spirochete exploit the molecular switch mechanism of the complement
594 protease C1s. J Biol Chem 298:102557.

595 49. Pereira MJ, Wager B, Garrigues RJ, Gerlach E, Quinn JD, Dowdell AS, Osburne MS,
596 Zückert WR, Kraiczy P, Garcia BL, Leong JM. 2022. Lipoproteome screening of the
597 Lyme disease agent identifies inhibitors of antibody-mediated complement killing. Proc
598 Natl Acad Sci U S A 119:e2117770119.
599 50. Babb K, McAlister JD, Miller JC, Stevenson B. 2004. Molecular characterization of
600 *Borrelia burgdorferi erp* promoter/operator elements. J Bacteriol 186:2745-56.
601 51. Miller JC, von Lackum K, Babb K, McAlister JD, Stevenson B. 2003. Temporal analysis
602 of *Borrelia burgdorferi* Erp protein expression throughout the mammal-tick infectious
603 cycle. Infect Immun 71:6943-52.
604 52. Burns LH, Adams CA, Riley SP, Jutras BL, Bowman A, Chenail AM, Cooley AE,
605 Haselhorst LA, Moore AM, Babb K, Fried MG, Stevenson B. 2010. BpaB, a novel
606 protein encoded by the Lyme disease spirochete's cp32 prophages, binds to *erp* Operator
607 2 DNA. Nucleic Acids Res 38:5443-55.
608 53. Jutras BL, Verma A, Adams CA, Brissette CA, Burns LH, Whetstine CR, Bowman A,
609 Chenail AM, Zuckert WR, Stevenson B. 2012. BpaB and EbfC DNA-binding proteins
610 regulate production of the Lyme disease spirochete's infection-associated Erp surface
611 proteins. J Bacteriol 194:778-86.
612 54. Jutras BL, Chenail AM, Carroll DW, Miller MC, Zhu H, Bowman A, Stevenson B. 2013.
613 Bpur, the Lyme disease spirochete's PUR domain protein: identification as a
614 transcriptional modulator and characterization of nucleic acid interactions. J Biol Chem
615 288:26220-34.

616 55. Casjens S, van Vugt R, Tilly K, Rosa PA, Stevenson B. 1997. Homology throughout the
617 multiple 32-kilobase circular plasmids present in Lyme disease spirochetes. J Bacteriol
618 179:217-27.
619 56. Barbour AG, Hayes SF, Heiland RA, Schrumpf ME, Tessier SL. 1986. A *Borrelia*-
620 specific monoclonal antibody binds to a flagellar epitope. Infect Immun 52:549-54.
621 57. Song X, Goedhart J. 2024. EzReverse – a Web Application for Background Adjustment
622 of Color Images. bioRxiv doi:10.1101/2024.05.27.594095:2024.05.27.594095.
623 58. Goedhart J, Luijsterburg MS. 2020. VolcaNoseR is a web app for creating, exploring,
624 labeling and sharing volcano plots. Scientific Reports 10.
625 59. Tang D, Chen M, Huang X, Zhang G, Zeng L, Zhang G, Wu S, Wang Y. 2023. SRplot:
626 A free online platform for data visualization and graphing. PLoS One 18:e0294236.
627 60. Si F, Li D, Cox SE, Sauls JT, Azizi O, Sou C, Schwartz AB, Erickstad MJ, Jun Y, Li X,
628 Jun S. 2017. Invariance of Initiation Mass and Predictability of Cell Size in *Escherichia*
629 *coli*. Curr Biol 27:1278-1287.
630 61. Myrbraten IS, Wiull K, Salehian Z, Havarstein LS, Straume D, Mathiesen G, Kjos M.
631 2019. CRISPR Interference for Rapid Knockdown of Essential Cell Cycle Genes in
632 *Lactobacillus plantarum*. mSphere 4.
633 62. Bjånes E, Stream A, Gibson PS, Bravo AM, Dahesh S, Baker JL, Varble A, Nizet V,
634 Veening J-W. 2024. An efficient *in vivo*-inducible CRISPR interference system for group
635 A *Streptococcus* genetic analysis and pathogenesis studies. bioRxiv
636 doi:10.1101/2024.02.22.581527:2024.02.22.581527.
637 63. Fenster JA, Werner AZ, Tay JW, Gillen M, Schirokauer L, Hill NC, Watson A, Ramirez
638 KJ, Johnson CW, Beckham GT, Cameron JC, Eckert CA. 2022. Dynamic and single cell

639 characterization of a CRISPR-interference toolset in *Pseudomonas putida* KT2440 for β-
640 ketoadipate production from p-coumarate. Metab Eng Commun 15:e00204.
641 64. Meunier A, Cornet F, Campos M. 2021. Bacterial cell proliferation: from molecules to
642 cells. FEMS Microbiol Rev 45.
643 65. Jutras BL, Scott M, Parry B, Biboy J, Gray J, Vollmer W, Jacobs-Wagner C. 2016. Lyme
644 disease and relapsing fever *Borrelia* elongate through zones of peptidoglycan synthesis
645 that mark division sites of daughter cells. Proc Natl Acad Sci U S A 113:9162-70.
646 66. Van De Putte P, Van D, Roersch A. 1964. The selection of mutants of *Escherichia coli*
647 with impaired cells division at elevated temperature. Mutat Res 106:121-8.
648 67. Wang H, Henk MC, Gayda RC. 1993. Overexpression of *ftsA* induces large bulges at the
649 septal regions in *Escherichia coli*. Current Microbiology 26:175-181.
650 68. Meisner J, Montero Llopis P, Sham LT, Garner E, Bernhardt TG, Rudner DZ. 2013.
651 FtsEX is required for CwlO peptidoglycan hydrolase activity during cell wall elongation
652 in *Bacillus subtilis*. Mol Microbiol 89:1069-83.
653 69. Li J, Xu X, Shi J, Hermoso JA, Sham L-T, Luo M. 2023. Regulation of the cell division
654 hydrolase RipC by the FtsEX system in *Mycobacterium tuberculosis*. Nature
655 Communications 14:7999.
656 70. Xu X, Li J, Chua W-Z, Pages MA, Shi J, Hermoso JA, Bernhardt T, Sham L-T, Luo M.
657 2023. Mechanistic insights into the regulation of cell wall hydrolysis by FtsEX and EnvC
658 at the bacterial division site. Proceedings of the National Academy of Sciences
659 120:e2301897120.
660 71. Du S, Pichoff S, Lutkenhaus J. 2016. FtsEX acts on FtsA to regulate divisome assembly
661 and activity. Proceedings of the National Academy of Sciences 113:E5052-E5061.

662 72. Diez AA, Farewell A, Nannmark U, Nyström T. 1997. A mutation in the *ftsK* gene of
663 *Escherichia coli* affects cell-cell separation, stationary-phase survival, stress adaptation,
664 and expression of the gene encoding the stress protein UspA. J Bacteriol 179:5878-83.
665 73. Liu G, Draper GC, Donachie WD. 1998. FtsK is a bifunctional protein involved in cell
666 division and chromosome localization in *Escherichia coli*. Mol Microbiol 29:893-903.
667 74. Steiner W, Liu G, Donachie WD, Kuempel P. 1999. The cytoplasmic domain of FtsK
668 protein is required for resolution of chromosome dimers. Mol Microbiol 31:579-83.
669 75. Crozat E, Rousseau P, Fournes F, Cornet F. 2014. The FtsK family of DNA translocases
670 finds the ends of circles. J Mol Microbiol Biotechnol 24:396-408.
671 76. Yu XC, Weihe EK, Margolin W. 1998. Role of the C terminus of FtsK in *Escherichia*
672 *coli* chromosome segregation. J Bacteriol 180:6424-8.
673 77. Capiaux H, Lesterlin C, Pérals K, Louarn JM, Cornet F. 2002. A dual role for the FtsK
674 protein in *Escherichia coli* chromosome segregation. EMBO Rep 3:532-6.
675 78. Aussel L, Barre FX, Aroyo M, Stasiak A, Stasiak AZ, Sherratt D. 2002. FtsK Is a DNA
676 motor protein that activates chromosome dimer resolution by switching the catalytic state
677 of the XerC and XerD recombinases. Cell 108:195-205.
678 79. Begg KJ, Dewar SJ, Donachie WD. 1995. A new *Escherichia coli* cell division gene,
679 *ftsK*. J Bacteriol 177:6211-22.
680 80. Grenga L, Luzi G, Paolozzi L, Ghelardini P. 2008. The *Escherichia coli* FtsK functional
681 domains involved in its interaction with its divisome protein partners. FEMS
682 microbiology letters 287:163-167.

683 81. Chen JC, Beckwith J. 2001. FtsQ, FtsL and FtsI require FtsK, but not FtsN, for co-
684 localization with FtsZ during *Escherichia coli* cell division. Molecular microbiology
685 42:395-413.
686 82. Sperandio V, Torres AG, Kaper JB. 2002. Quorum sensing *Escherichia coli* regulators B
687 and C (QseBC): a novel two-component regulatory system involved in the regulation of
688 flagella and motility by quorum sensing in *E. coli*. Mol Microbiol 43:809-21.
689 83. Rollend L, Fish D, Childs JE. 2013. Transovarial transmission of *Borrelia* spirochetes by
690 *Ixodes scapularis*: a summary of the literature and recent observations. Ticks Tick Borne
691 Dis 4:46-51.
692 84. Zhao X, Zhang K, Boquoi T, Hu B, Motaleb MA, Miller KA, James ME, Charon NW,
693 Manson MD, Norris SJ, Li C, Liu J. 2013. Cryoelectron tomography reveals the
694 sequential assembly of bacterial flagella in *Borrelia burgdorferi*. Proc Natl Acad Sci U S
695 A 110:14390-5.
696 85. Qin Z, Tu J, Lin T, Norris SJ, Li C, Motaleb MA, Liu J. 2018. Cryo-electron tomography
697 of periplasmic flagella in *Borrelia burgdorferi* reveals a distinct cytoplasmic ATPase
698 complex. PLoS Biol 16:e3000050.
699 86. Chang Y, Moon KH, Zhao X, Norris SJ, Motaleb MA, Liu J. 2019. Structural insights
700 into flagellar stator–rotor interactions. eLife 8:e48979.
701

Figure Legends.

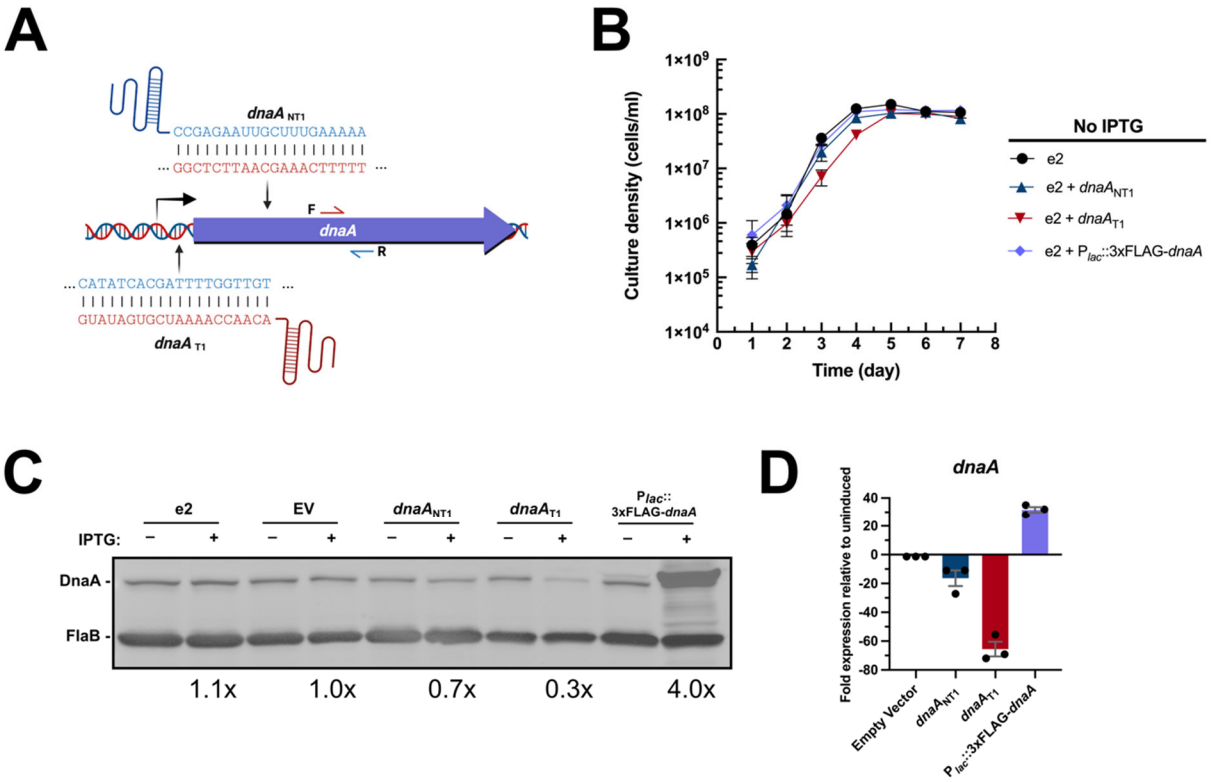

Figure 1. Validation of conditional dysregulation of DnaA. (A) Two sgRNAs were designed to knock down borrelial *dnaA* transcription by CRISPRi. One sgRNA targeted the template strand directly upstream of the ORF (*dnaA*$_{T1}$), while the other targeted the template strand within the ORF (*dnaA*$_{NT1}$). **(B)** The *dnaA* CRISPRi bacteria, CRISPRi empty vector bacteria, and the strain with the *dnaA* overexpression plasmid grew at the same rate as the parental e2. Adding IPTG to these strains resulted in appropriate knockdown or overexpression of DnaA protein **(C)** and transcript **(D)**, as assessed by immunoblot and qRT-PCR. The overexpression shuttle vector encodes a DnaA with an N-terminal 3xFLAG moiety and thus migrates above the native protein.

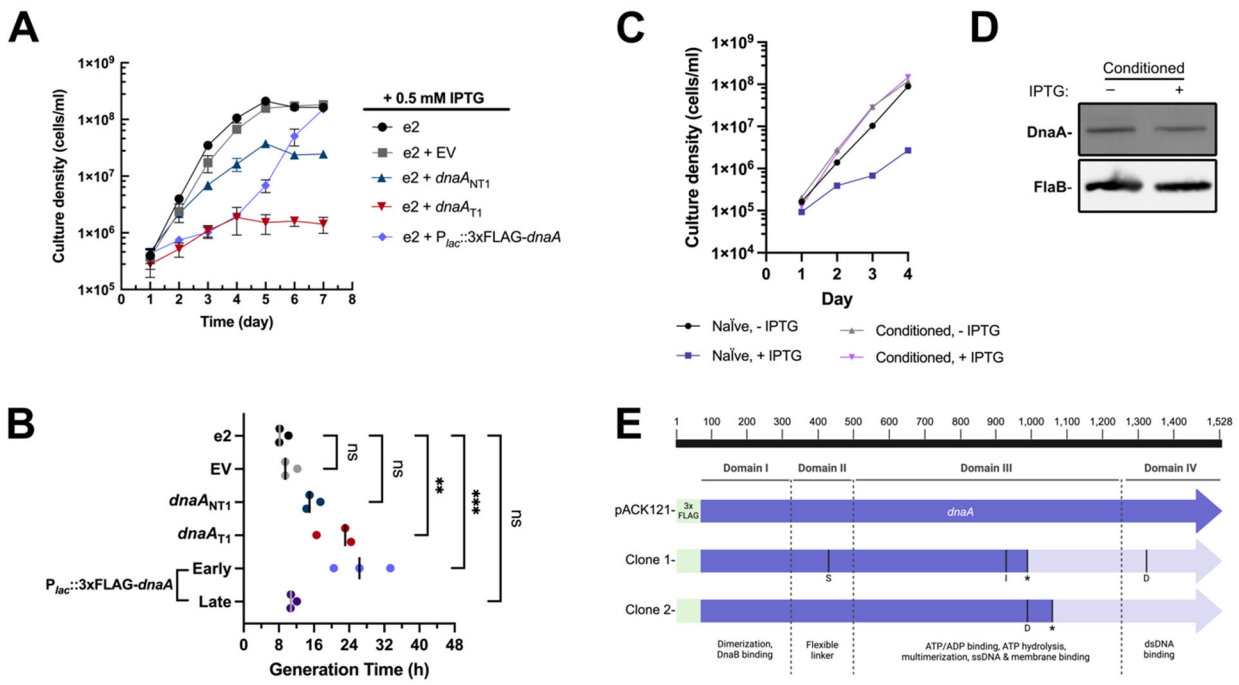

Figure 2. Appropriate expression of DnaA is required for *B. burgdorferi* replication. (A) Growth curve studies were conducted on different *B. burgdorferi* e2 strains incubated with 0.5 mM IPTG. **(B)** The generation time was determined from three individual cultures of each strain. Three independent cultures of each strain were measured for growth curve analysis. For the overexpression strain, the growth rate was determined before (early; 1-4 dpi) and after the resumption of growth (late; 4-7 dpi). The resumption of replication in that strain was evidently due to mutation of the overexpressed *dnaA* gene. **(C)** IPTG-treated DnaA overexpression spirochetes that resumed growth (conditioned) lost sensitivity to IPTG when passaged to fresh media and did not produce 3xFLAG-DnaA as assessed by immunoblot **(D)**, supporting the conclusion that accumulated mutations in the overexpression *dnaA* permitted replication. **(E)** Sequencing plasmid from these conditioned spirochetes showed unique mutations (S = substitution; D = deletion) in the 3xFLAG-*dnaA* ORF that caused a frameshift and truncation of the full-length protein.

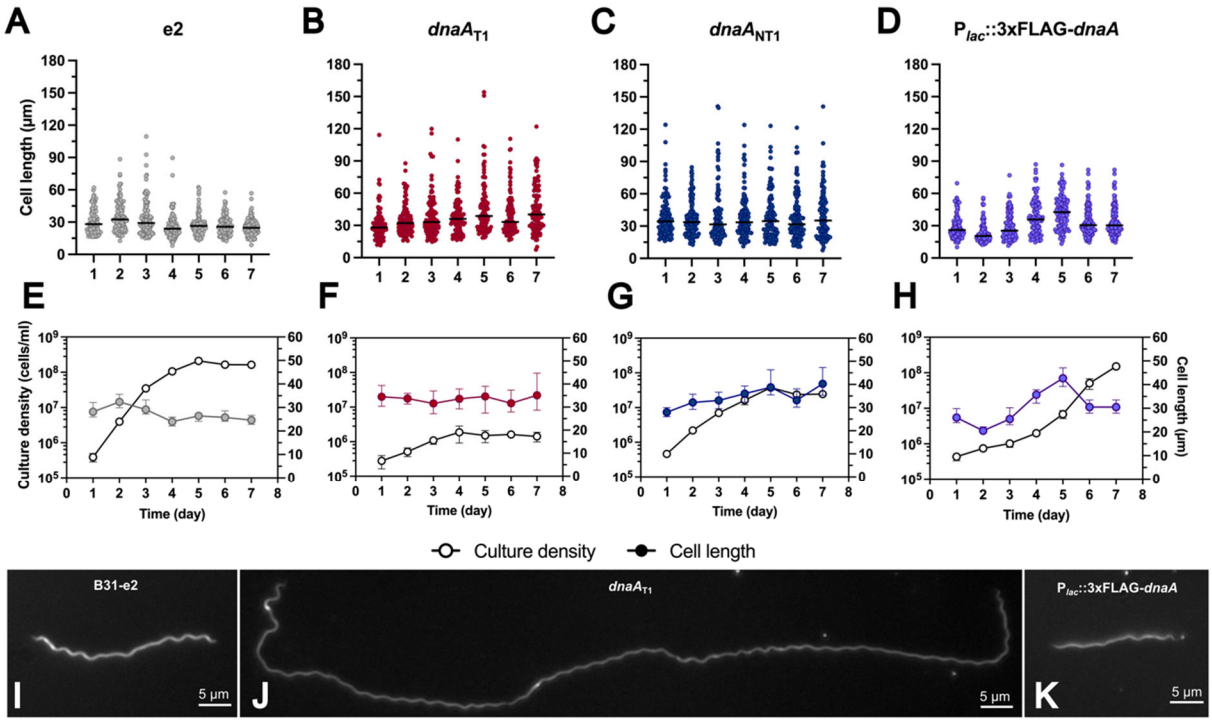

Figure 3. DnaA dysregulation affects spirochete cell length. (A-D) Cell lengths of the 0.5 mM IPTG-treated *B. burgdorferi* e2 strains measured over seven days (gray = e2; red = *dnaA*$_{T1}$; *dnaA*$_{NT1}$ = blue; P$_{lac}$::3xFLAG-*dnaA* = purple). The line represents the median cell length. **(E-H)** The median cell length with the 95% CI (filled-in circle) superimposed against the corresponding growth curve (empty circle) from Fig. 2. **(I-K)** Representative images of observed phenotypes. **(I)** The e2 cell has a median length of 2 dpi. **(J)** DnaA-depleted cell with the characteristic elongation phenotype. **(K)** Median size of a DnaA overexpression spirochete after 2 dpi.

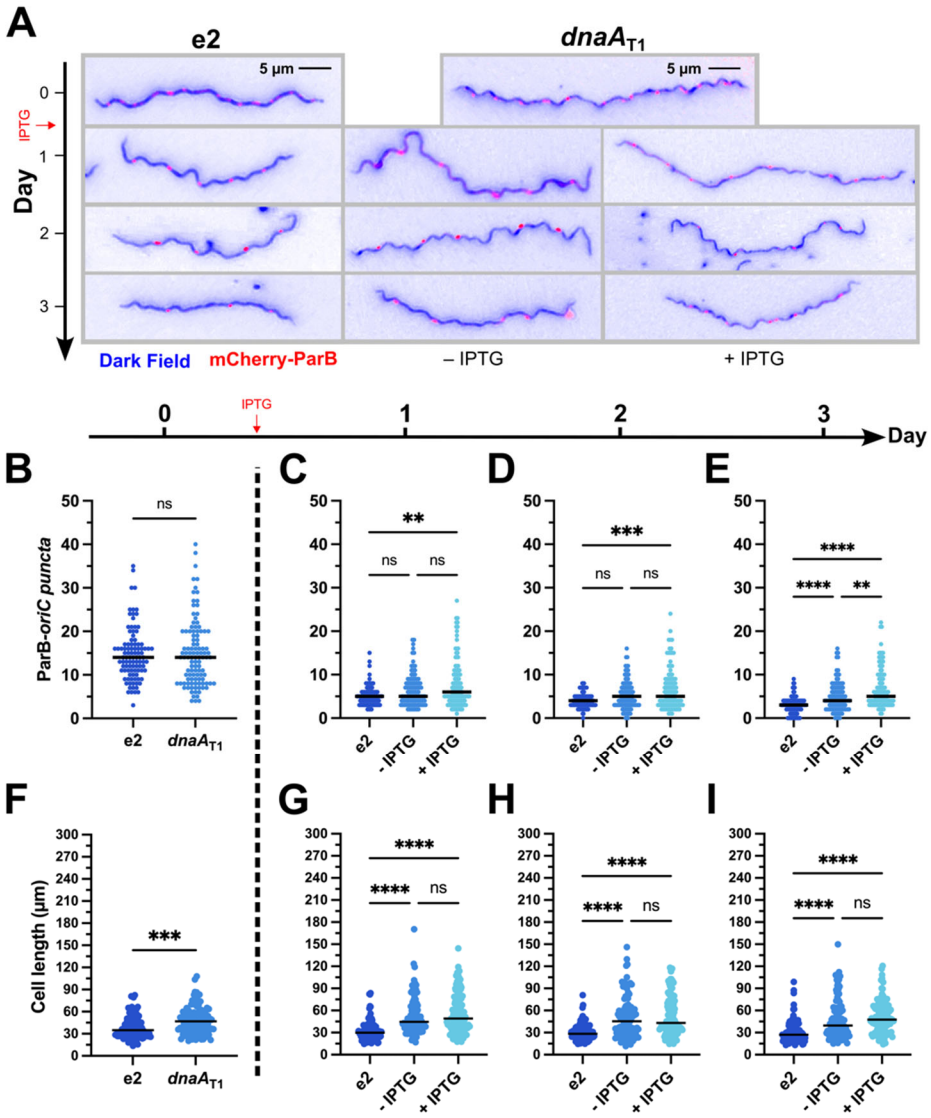

Figure 4. Knockdown of DnaA increases the number of chromosomes per spirochete. The *B. burgdorferi* CRISPRi *dnaA*$_{T1}$ and parent e2 strains were transformed with a construct encoding a mCherry-tagged ParB protein, which binds near the *oriC*, to identify the locations of the chromosomes. The two strains were grown without inducer until mid-log (t = 0), and then the *dnaA*$_{T1}$ strain was divided into two cultures, and one of those was induced with 0.5 mM IPTG. Cultures were tracked for three more days. **(A)** Representative merged micrographs (blue = dark field; red = mCherry-ParB) of spirochetes with the approximate median numbers of ParB-*oriC*

745 puncta **(B)** and cell length **(C)**. Significant differences in puncta and cell length at day 0 were
746 determined by the Mann-Whitney test. Differences between the three groups (e2, - IPTG, and +
747 IPTG) on days 1-3 were tested for by the Kruskal-Wallis test and then Dunn's test for multiple
748 comparisons. Multiplicity-adjusted p-values are reported. **, $p \leq 0.01$; ***, $p \leq 0.001$; ****, $p \leq$
749 0.0001; ns, not significant, $p > 0.05$. Approximately 50 spirochetes were imaged for each strain on
750 each day. Data were gathered from two independent experiments.

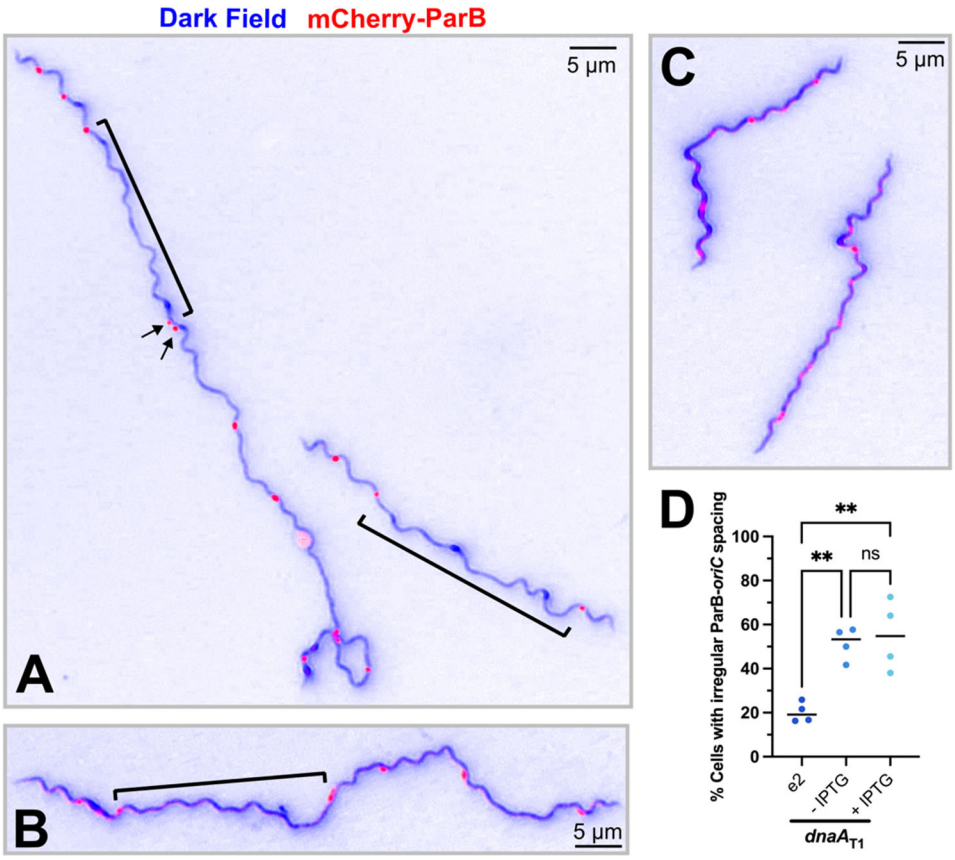

Figure 5. Irregular spacing of *oriC* in *dnaA* knockdown *B. burgdorferi*. (A-B) Representative images of spirochetes containing the *dnaA*$_{T1}$ CRISPRi plasmid with irregular spacing of ParB-*oriC* puncta (red). DnaA-deplete cells had large regions where not foci were observed (white brackets). Some cells also had foci that were close together (arrows). **(C)** Parental e2 spirochetes with approximately the same number of ParB-*oriC* puncta as the mutant but exhibit regular oriC spacing. **(D)** The number of spirochetes with irregular ParB-*oriC* was quantified (e2, n = 184; uninduced *dnaA*$_{T1}$, n = 198 cells; induced *dnaA*$_{T1}$ n = 206). One-way ANOVA with Tukey's post hoc test was done to determine the significance and make comparisons. The multiplicity-adjusted p-values are reported **, $p \leq 0.01$; ns, not significant, $p > 0.05$.

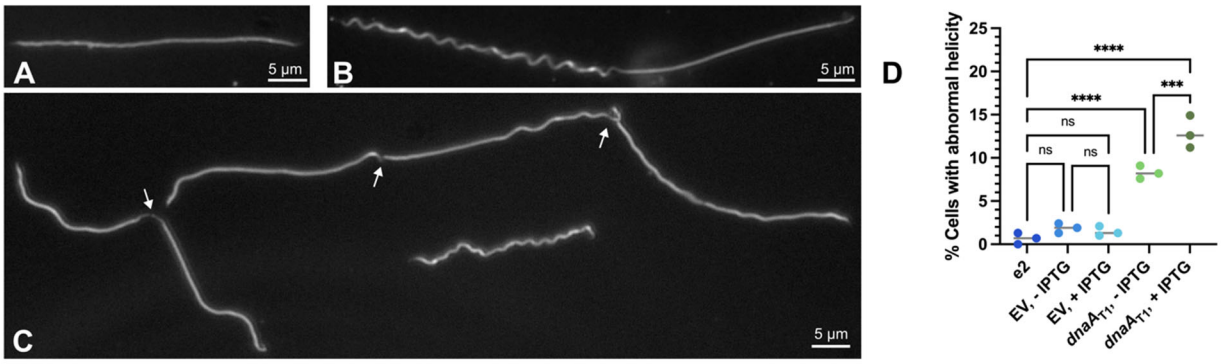

Figure 6. DnaA-depletion affects borrelial helicity. Representative micrographs of observed phenotypes. When *dnaA* was knocked down, spirochetes with no **(A)** or asymmetrical helicity **(B)** were observed. **(C)** Some of the abnormal cells were elongated and showed division defects. **(D)** Spirochetes exhibiting similar defects were observed at a low level in the e2 strain (0.7%, n = 1514). The empty vector (EV) control cultures had a similar proportion, independent of the addition of IPTG (uninduced: 2.1%, n = 1439; induced: 1.6%, n = 1608). The bacteria with the *dnaA*$_{T1}$ CRISPRi plasmid had significantly more cells with perturbed helicity that was dependent on induction (uninduced: 8.7%, n = 1437; induced: 13%, n = 1472). Spirochetes were counted from three independent cultures. Statistical significance was determined by one-way ANOVA with a Holm-Šídák's post-hac test, and multiplicity-adjusted p-values are reported. ***, $p \leq 0.001$, ****, $p \leq 0.0001$; ns, not significant, $p > 0.05$.

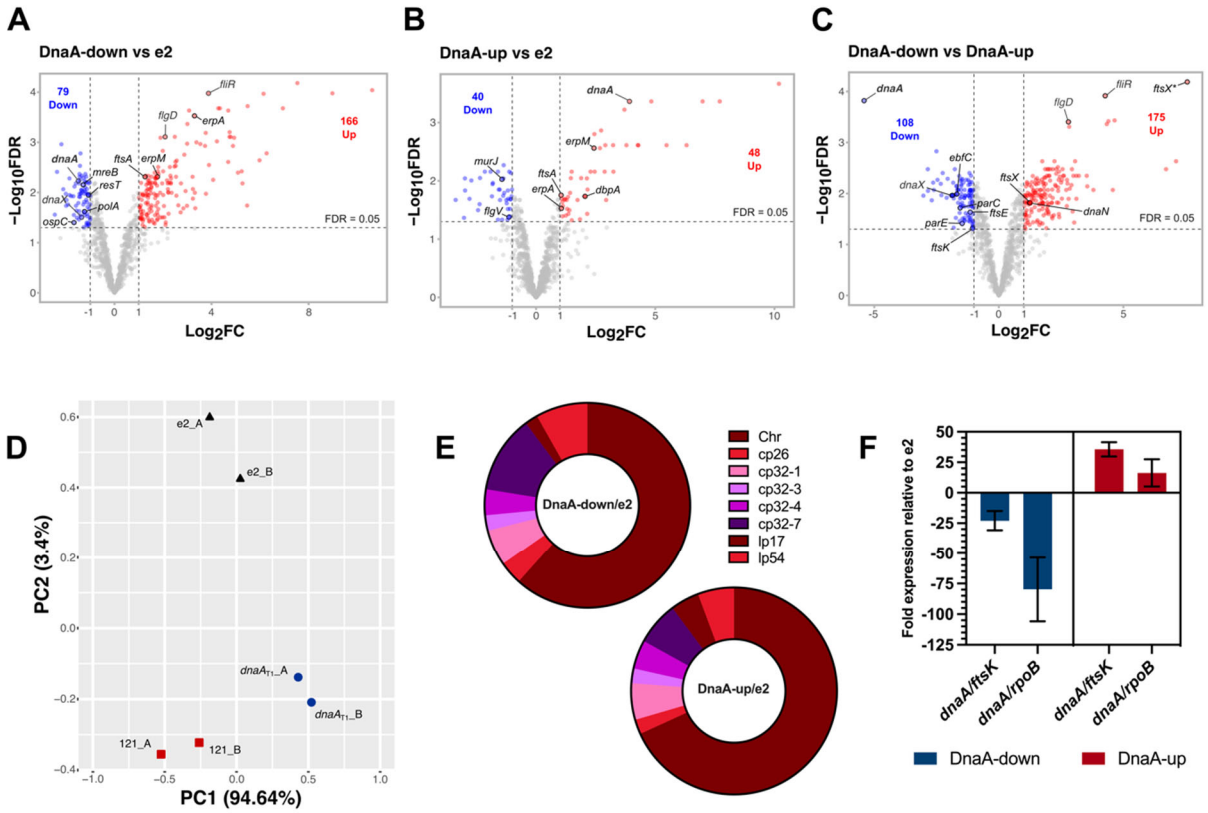

Figure 7. RNA-seq of DnaA-dysregulated *B. burgdorferi*. The RNA from three *B. burgdorferi* strains with different cellular levels of DnaA were sequenced: e2 (parent), CRISPRi *dnaA*$_{T1}$ (DnaA-down), and overexpression pACK121 (DnaA-up). **(A-C)** Volcano plots plotting the fold change ($\log_2$FC) against each gene's false discovery rate (-log(FDR)). The threshold for significance was set at a $\log_2$FC ≥ 1 or ≤ - 1 (≥ 2-fold change) and an FDR of ≤ 0.05. **(D)** PCA plot showing the clustering of the replicate samples that were sequenced. **(E)** Donut charts showing the replicon on which the significantly affected genes are encoded. **(F)** qRT-PCR results of *dnaA* transcripts in the sequenced samples. Cq values were normalized to *ftsK* or *rpoB* (ΔCq) and then to the parental strain (ΔΔCq).

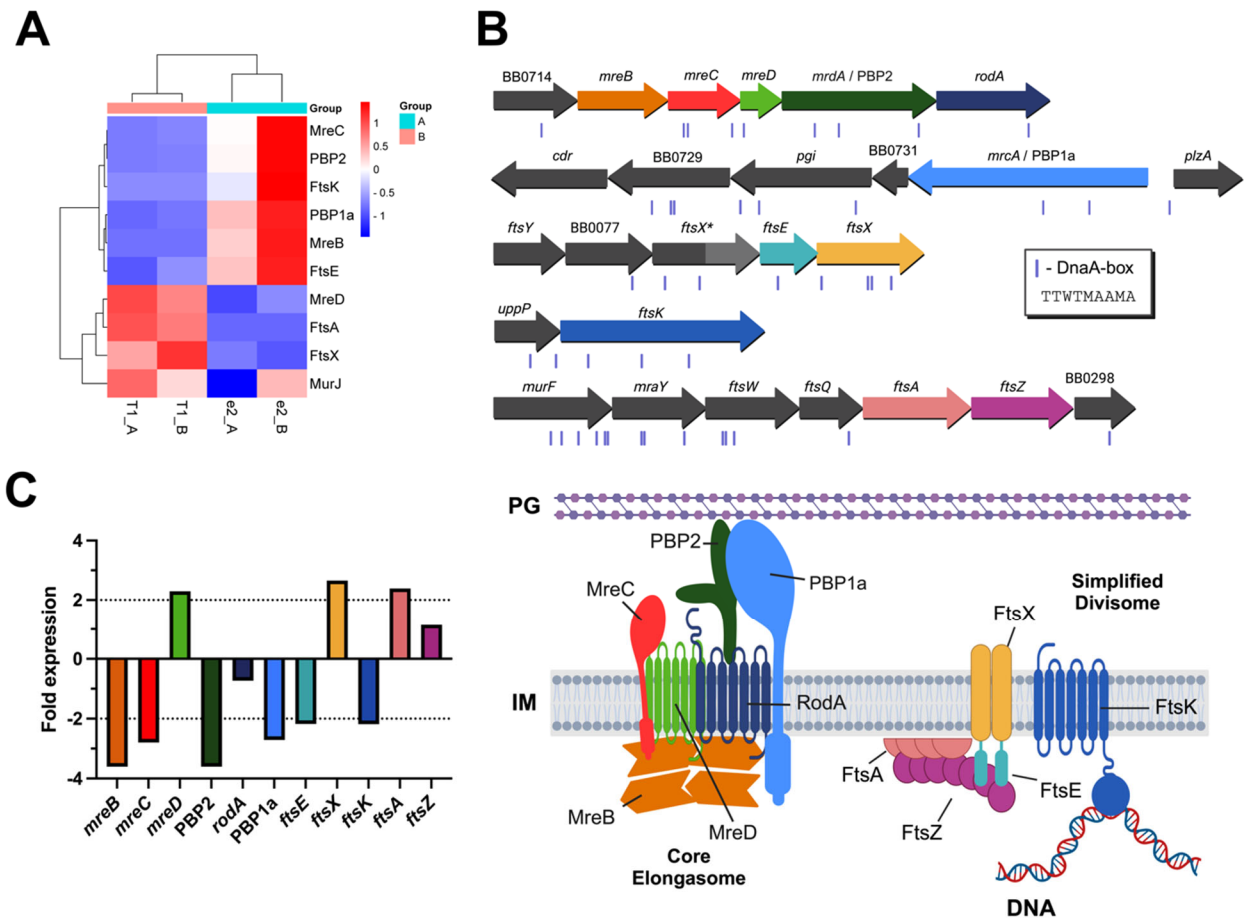

Figure 8. Impacts of DnaA on *B. burgdorferi* elongation and division genes. (A) Heat map of the division and elongation genes that were significantly affected when DnaA was knocked down. **(B)** Top: Locus maps of the select elongation and division genes to scale. The sites of potential DnaA-boxes are denoted as purple boxes below the genes. Bottom: Simplified schema of the hypothesized borrelial elongasome and divisome containing the highlighted genes of interest. Informed by the work of Liu et al. and Hu et al. (35, 71) **(C)** Bar graph showing the fold change detected by RNA-seq of the elongation and division genes. The dashed lines indicate the cut-off for significance.

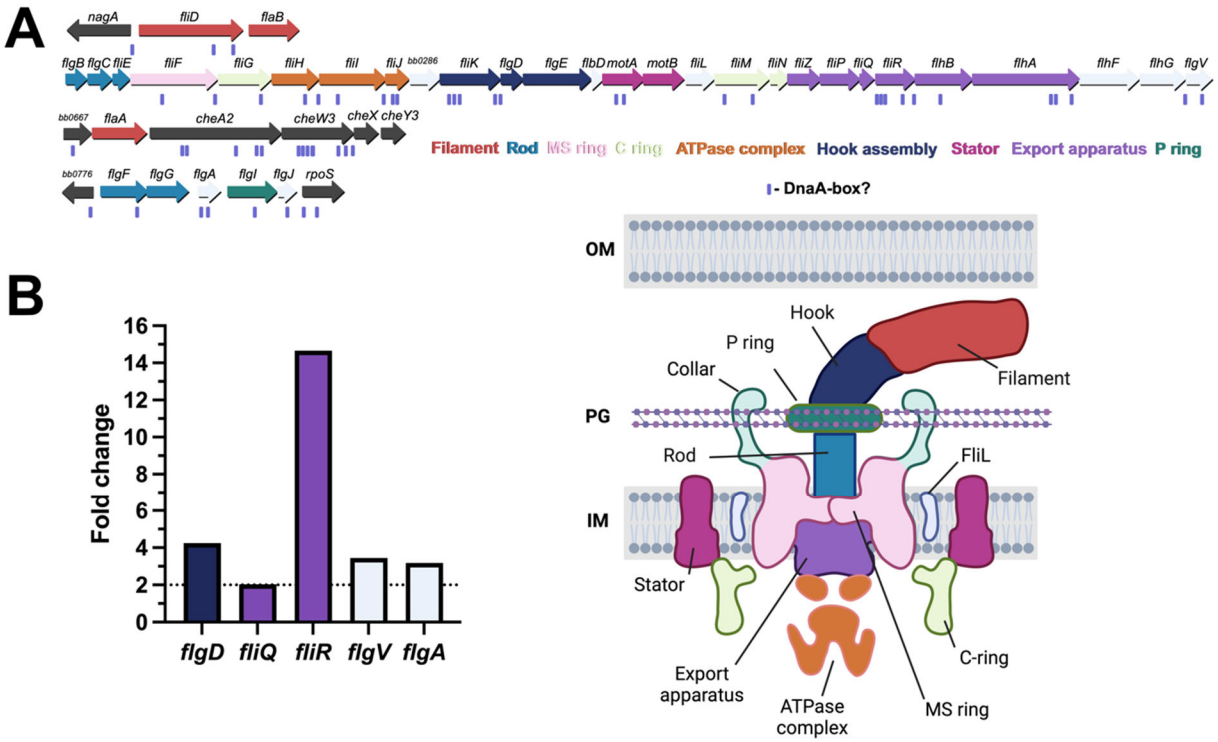

Figure 9. Impacts of DnaA on *B. burgdorferi* flagellar genes. (A) The borrelial flagellar motor is a complex molecular machine (bottom right) that is comprised of nearly three dozen proteins encoded in four separate loci on the chromosome (top). The schematic of the *B. burgdorferi* flagellar motor was informed from data by Zhao et al., Qin et al., and Chang et al. (84-86). **(B)** RNA-seq showed the transcripts for five flagellar genes increased when DnaA was knocked down. Two of these genes, FliQ and FliR (purple), are constituents of the flagellar export apparatus. The dashed line indicates the cut-off for significance.

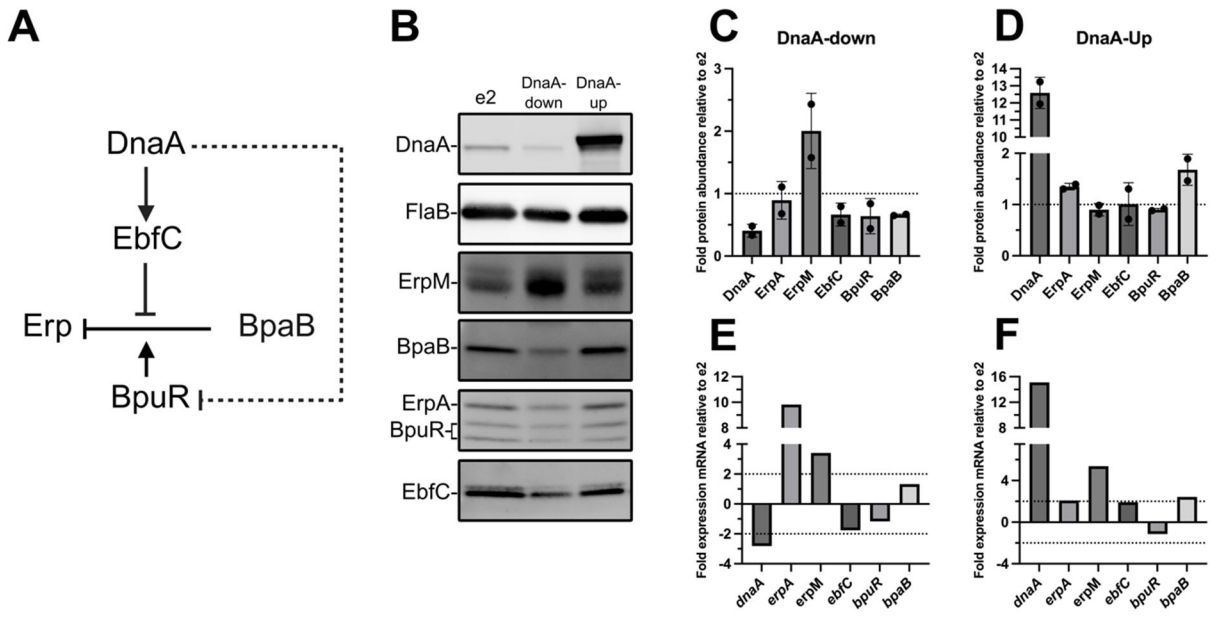

Fig. 10. Impacts of DnaA on the Erp regulatory network. (A) Solid black lines indicate established interactions. Dashed lines indicate hypothesized interactions. Activation is denoted by lines with arrowheads, and inhibition by lines without arrowheads. Note that co-repressive or anti-repressive activities, i.e., BpuR and EbfC, respectively, are indicated by arrows directed at lines. **(B)** Representative immunoblots from samples of *B. burgdorferi* that were analyzed by RNA-seq. Quantitation of target proteins when DnaA was knocked down **(C)** or overexpressed **(D)**. Band intensities for each replicate immunoblot were normalized to FlaB and then the parental e2 strain. **(C-D)** The dotted lines at 1 represent where the protein abundance is the same as e2. Bar graphs showing the fold change detected by RNA-seq in the DnaA-down/e2 **(E)** and DnaA-up comparisons **(F)**. **(E-F)** The dotted lines indicate the 2-fold threshold for significance.

823 **Table 1.** Homologous elongation and division genes of *B. burgdorferi*.

				RNA-seq Differential Expression		
Protein	**Locus Tag**	**Elongasome**	**Divisome**	**DnaA-down vs e2**	**DnaA-up vs e2**	**DnaA-down vs DnaA-up**
FtsE	BB_0080	-	+	Down	NA	Down
FtsX	BB_0081	-	+	Up	NA	Up
FtsI	BB_0136	+	+	NA	NA	NA
MurE	BB_0201	+	+	NA	NA	NA
FtsK	BB_0257	-	+	NA	NA	Down
FtsZ	BB_0299	-	+	NA	NA	NA
FtsA	BB_0300	-	+	Up	Up	NA
FtsQ/DivlB	BB_0301	-	+	NA	NA	NA
FtsW	BB_0302	-	+	NA	NA	NA
MraY	BB_0303	+	+	NA	NA	NA
MurF	BB_0304	+	+	NA	NA	NA
MurB	BB_0585	+	+	NA	NA	NA
MurD	BB_0585	+	+	NA	NA	NA
Ami	BB_0666	-	+	NA	NA	NA
MreB	BB_0715	+	-	Down	NA	Down
MreC	BB_0716	+	-	Down	NA	Down
MreD	BB_0717	+	-	Up	NA	Down
PBP2	BB_0718	+	-	Down	NA	Down
RodA	BB_0719	+	-	NA	NA	NA
PBP1a	BB_0732	+	-	Down	NA	Down
MurG	BB_0767	+	+	NA	NA	NA
MurJ	BB_0810	+	+	NA	Down	Up
MurC	BB_0817	+	+	NA	NA	NA

824 * Plus sign (+) indicates the protein is part of the complex, minus sign (-) indicates it is not
825 * NA = Not affected
826

827 **Table 2.** Oligonucleotides used in this study.

Target	Name	Sequence	Purpose	Source
dnaA ORF	qPCR *dnaA* F	CATGTGACCGATCTCCTTCTG	qPCR	(10)
	qPCR *dnaA* R	CGACAATAGCTGCTCTGAGTT		
ftsK ORF	qPCR *ftsK* F	GACCTTCTGATGAGCCAATGT	qPCR	(10)
	qPCR *ftsk* R	GCTGCTCTGTTGTAACCTATCT		
rpoB ORF	qPCR *rpoB* F	GTTCATCTGGGACAAGGAAGAG	qPCR	This study
	qPCR *rpoB* R	CAGACTCAAGGCCCTCATTAAG		

828